Kinetic and Spectroscopic Characterization of the Gamma-Carbonic Anhydrase from the Methanoarchaeon *Methanosarcina thermophila*[†]

Birgit E. Alber,[‡] Christopher M. Colangelo,[§] Jun Dong,[§] Christina M. V. Stålhandske,[§] Teaster T. Baird,[||] Chingkuang Tu,[⊥] Carol A. Fierke,[||] David N. Silverman,[⊥] Robert A. Scott,[§] and James G. Ferry*,[‡]

Department of Biochemistry and Molecular Biology, The Pennsylvania State University, University Park, Pennsylvania, 16802, Center for Metalloenzyme Studies, University of Georgia, Athens, Georgia 30602, Department of Biochemistry, Duke University Medical Center, Durham, North Carolina, 27710, and Department of Pharmacology and Therapeutics, University of Florida, College of Medicine, Gainesville, Florida, 32610

Received December 8, 1998; Revised Manuscript Received July 21, 1999

ABSTRACT: The zinc and cobalt forms of the prototypic γ-carbonic anhydrase from *Methanosarcina thermophila* were characterized by extended X-ray absorption fine structure (EXAFS) and the kinetics were investigated using steady-state spectrophotometric and ^{18}O exchange equilibrium assays. EXAFS results indicate that cobalt isomorphously replaces zinc and that the metals coordinate three histidines and two or three water molecules. The efficiency of either Zn−Cam or Co−Cam for CO_2 hydration (k_{cat}/K_m) was severalfold greater than HCO_3^- dehydration at physiological pH values, a result consistent with the proposed physiological function for Cam during growth on acetate. For both Zn− and Co−Cam, the steady-state parameter k_{cat} for CO_2 hydration was pH-dependent with a pK_a of 6.5−6.8, whereas k_{cat}/K_m was dependent on two ionizations with pK_a values of 6.7−6.9 and 8.2−8.4. The ^{18}O exchange assay also identified two ionizable groups in the pH profile of k_{cat}/K_m with apparent pK_a values of 6.0 and 8.1. The steady-state parameter k_{cat} (CO_2 hydration) is buffer-dependent in a saturable manner at pH 8.2, and the kinetic analysis suggested a ping-pong mechanism in which buffer is the second substrate. The calculated rate constant for intermolecular proton transfer is 3×10^7 M^{-1} s^{-1}. At saturating buffer concentrations and pH 8.5, k_{cat} is 2.6-fold higher in H_2O than in D_2O, suggesting that an intramolecular proton transfer step is at least partially rate-determining. At high pH (pH > 8), k_{cat}/K_m is not dependent on buffer and no solvent hydrogen isotope effect was observed, consistent with a zinc hydroxide mechanism. Therefore, at high pH the catalytic mechanism of Cam appears to resemble that of human CAII, despite significant structural differences in the active sites of these two unrelated enzymes.

Carbonic anhydrases catalyze the reversible hydration of carbon dioxide (eq 1) and are ubiquitous in all three phylogenetic domains of life: the Archaea, Eucarya, and Bacteria.

$$CO_2 + H_2O \rightleftarrows HCO_3^- + H^+ \qquad (1)$$
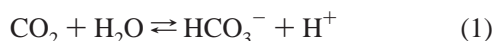
On the basis of sequence comparisons, there are three distinct classes (α, β, and γ) that appear not to share a common ancestor (*1−3*). All three classes contain a catalytic zinc ion that has been structurally characterized by EXAFS[1] for both the α (*4*) and β (*5, 6*) classes, but not the γ class. Although a crystal structure has not been reported for the β class, EXAFS indicates that the zinc atom is coordinated to one histidine, two cysteines, and one to two solvent molecules. Crystal structures have been determined for five isozymes (I−V) of the monomeric human carbonic anhydrase belonging to the α class (*7−11*). The crystal structure has also been determined for the trimeric Cam from the methanoarchaeon *Methanosarcina thermophila* (*12*). Cam is the prototype of the γ class and the only procaryotic carbonic anhydrase for which a structure is known. The drastic departure in the tertiary and quaternary structure of Cam compared to the human isozymes provides further evidence that the α- and γ-classes did not evolve from a common ancestor, yet the

* To whom correspondence should be addressed. Telephone: 814-863-5721. Fax: 814/863-6217. E-mail:jgf3@psu.edu.
[‡] Department of Biochemistry and Molecular Biology, The Pennsylvania State University.
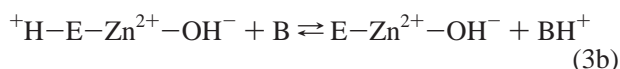[§] Center for Metalloenzyme Studies, University of Georgia.
[||] Department of Biochemistry, Duke University Medical Center.
[⊥] Department of Pharmacology and Therapeutics, University of Florida.

[1] Abbreviations: EXAFS, extended X-ray absorption fine structure; Cam, *Methanosarcina thermophila* carbonic anhydrase produced in *Escherichia coli*; apo-Cam, metal-depleted Cam; Zn−Cam, zinc-reconstituted apo-Cam; Co−Cam, cobalt-reconstituted apo-Cam; MES, 2-(*N*-morpholino) ethanesulfonic acid; TAPS, *N*-tris(hydroxymethyl)-methyl-3-aminopropanesulfonic acid; MOPS, 2-(*N*-morpholino)propanesulfonic acid; HEPES, 4-(2-hydroxyethyl)-1-piperazineethanesulfonic acid; XAS X-ray absorption spectroscopy.

α- and γ-carbonic anhydrases contain a catalytically essential zinc ion coordinated by three histidine residues. This conserved structural feature suggests convergent evolution of the catalytic mechanism; however, residues adjacent to zinc in the active sites of Cam and the human isozymes bear little resemblance (*12, 13*). Several mammalian isozymes from the α class have been studied in great detail and follow a common "zinc-hydroxide" mechanism for catalysis (*14−17*). The overall enzyme-catalyzed reaction occurs in two mechanistically distinct half-reactions. The first half-reaction is the interconversion of carbon dioxide and bicarbonate (eqs 2a and 2b) that is reflected in the steady-state parameter k_{cat}/K_m. The second half-reaction contains the rate-determining intramolecular and intermolecular proton-transfer steps (eqs 3a and 3b) that are reflected in the steady-state parameter k_{cat}.

$$E-Zn^{2+}-OH^- + CO_2 \rightleftarrows E-Zn^{2+}-HCO_3^- \quad (2a)$$

$$E-Zn^{2+}-HCO_3^- + H_2O \rightleftarrows$$
$$E-Zn^{2+}-H_2O + HCO_3^- \quad (2b)$$

$$E-Zn^{2+}-H_2O \rightleftarrows {}^+H-E-Zn^{2+}-OH^- \quad (3a)$$

$${}^+H-E-Zn^{2+}-OH^- + B \rightleftarrows E-Zn^{2+}-OH^- + BH^+ \quad (3b)$$
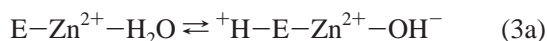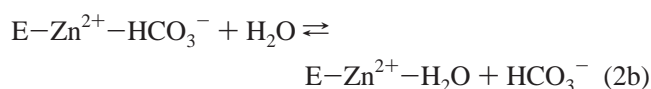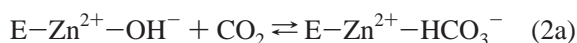
The group that shuttles protons between the active site to the surrounding medium was identified as His64 in the human isozymes CAII and CAIV (*18, 19*). Intramolecular proton transfer (eq 3a) is rate-limiting at saturating buffer concentrations, and at low buffer concentrations intermolecular proton transfer (eq 3b) is rate-limiting. Kinetic studies on the oligomeric spinach and pea carbonic anhydrases from the β class suggest that they also have a zinc hydroxide mechanism, although proton transfer from the active site to buffer appears to have changed (*6, 20, 21*).

Although the gene encoding Cam is part of an orthologous group (*22*) with representatives in all three phylogenetic domains (*3*), Cam is the only member for which a biochemical function has been assigned and a crystal structure determined; however, the kinetic mechanism has not yet been investigated. Here, we report on the first spectroscopic and kinetic characterization of Cam, which is also the first procaryotic carbonic anhydrase to be characterized in this detail.

EXPERIMENTAL PROCEDURES

Metal Substitution and Native Molecular Mass Determination. The *cam* gene (excluding a putative signal peptide) encoding carbonic anhydrase from *M. thermophila* was expressed in *Escherichia coli* and the heterologously produced enzyme (Cam) was purified as described previously (*23*). Apo-Cam was prepared using an ultrafiltration unit fitted with a YM10 membrane (Amicon, Beverly, MA). All solutions were prepared in plasticware using deionized water (18 MΩ) and all procedures were carried out at room temperature, unless otherwise indicated. Purified Cam (100−150 mg) was concentrated to 2−3 mL, and 8 mL of 8 M guanidine·HCl, 125 mM dipicolinic acid, 20 mM potassium phosphate (pH 6.2) were added. After 1 h, 100 mL of 100

Table 1: X-ray Absorption Spectroscopic Data Collection and Reduction for the As-Isolated (Zn-Containing) Cam and Co−Cam from *Methanosarcina thermophila*

element	Zn	Co
SR facility	SSRL	SSRL
beamline	7−3	7−3
monochromator crystal	Si[220]	Si[220]
detection method	Fluorescence	fluorescence
detector type	solid state array[a]	solid state array[a]
scan length, min	23	27
scans in average	12	6
temperature, K	10	10
energy standard	Zn foil	Co foil
	(first inflection)	(first infection)
energy calibration, eV	9659	7709
E_0, eV	9670	7715
preedge background	9333−9625	7384−7670
energy range, eV	8720	6930
Gaussian center, eV	1000	1125
Width, eV	9670−9881 (4)	7715−7918 (4)
spline background	9905−10 093 (4)	7928−8121 (4)
energy range, eV (polynomial order)	10 093−10 305 (3)	8121−8325 (3)

[a] The 13-element Ge solid-state X-ray fluorescence detector at SSRL is provided by the NIH Biotechnology Research Resource.

mM dipicolinic acid and 15 mM potassium phosphate (pH 6.3) was passed over the enzyme solution at a flow rate of 10 mL/hour. The protein was concentrated to 5 mL, and 100 mL of 20 mM potassium phosphate (pH 7.0) was passed over it. Apo-Cam was concentrated to 20−50 mg/mL and stored at −20 °C. Metal-reconstituted apo-Cam was prepared using the ultrafiltration unit (flow rate 10 mL/hour), and 100 mL of 20 mM potassium phosphate (pH 7.0) containing either 1 mM CoCl$_2$ or 1 mM ZnSO$_4$, followed by 100 mL of 20 mM potassium phosphate (pH 7.0). A Superose 12 (Pharmacia) gel filtration column calibrated with RNase A (13.7 kDa), chymotrypsinogen (25 kDa), ovalbumin (43 kDa), and bovine serum albumin (67 kDa; dimer, 134 kDa) was used to remove remaining unbound metals and to determine the native molecular mass of Cam, apo-Cam, Zn−Cam, and Co−Cam. Protein samples (0.2 mL, containing 24.9 to 25.7 mg enzyme) were injected onto the column equilibrated with 50 mM potassium phosphate (pH 7.0) containing 150 mM NaCl. The column was developed at a flow rate of 0.4 mL/min.

Visible and X-ray Absorption Spectroscopy. Optical absorption spectra of the Zn− and Co−Cam were collected at 25 °C using a Beckman DU640 spectrometer. For X-ray absorption spectroscopy (XAS), about 160−180 μL of Cam (41 mg/mL in 20 mM potassium phosphate (pH 7.0) containing 20% glycerol) were transferred to a Lucite cuvett covered with Mylar adhesive tape as an X-ray transparent window material, capped, and dropped into liquid nitrogen. Both Zn and Co K-edge XAS date of Cam were collected on beam line 7−3 at SSRL with SPEAR ring running at 3.0 GeV and 60−70 mA current (*24*). Details of XAS data collection and reduction are summarized in Table 1. Standard EXAFS analysis was performed (*24*) using EXAFSPAK software (http://ssr101.slac.stanford.edu/exafspak.html). Both single- and multiple-scattering paths 4.5 Å from the metal atom were used to identify and quantify imidazole coordination due to histidine. Multiple-scattering paths were built by taking the crystal structure of tetrakis(imidazole) zinc(II) perchlorate (*25*) or hexakis(imidazole) cobalt(II) nitrate (*26*)

and importing it into Ball & Stick software (v. 3.5, Cherwell Scientific). The model was edited to only the metal atom and one imidazole and the coordinates were then imported into FEFF v. 5.05 software (25−27) to calculate scattering amplitudes and phase shifts for each scattering path containing four or fewer legs. A constrained fitting process was then used with the following parameters. Coordination numbers were constrained to be integer values. The distances and Debye−Waller factors for outer-shell atoms of imidazole rings were constrained to a given ratio with first-shell (metal-nitrogen/oxygen) distance and Debye−Waller factor, respectively. In many fits, the first coordination sphere contains imidazole nitrogens plus additional nonimidazole(N/O)-containing ligands. Separating these into two shells with independent M-(N/O) distances had no more than a small effect on the fits. If separation improved the goodness-of-fit statistic, then these are reported. If not, then fits in which a single M-(N/O) distance was used for both imidazole and nonimidazole ligands are reported. First-shell distances are expected to be accurate to within 0.02 Å. The bond valence sum method was applied to EXAFS fits using standard procedures (27−29).

Steady-State Kinetic Measurements. Initial rates of CO_2 hydration and HCO_3^- dehydration were determined by stopped-flow spectroscopy (KinTek stopped flow apparatus, State College, PA) at 25 °C using the changing pH-indicator method (30). The following buffer/indicator pairs (and wavelengths) were used: at pH 5.5−6.8, MES (pK_a = 6.1)/chlorophenol red (574 nm); at pH 6.8−7.5, MOPS (pK_a = 7.2)/*p*-nitrophenol (400 nm); at pH 7.8, HEPES (pK_a = 7.5)/phenol red (557 nm); at pH 8.0−9.0, TAPS (pK_a = 8.4)/*m*-cresol purple (578 nm). The buffer concentration was 50 mM, and the ionic strength was maintained at 0.1 M by addition of sodium sulfate. Saturated solutions of CO_2 (33.8 mM) were prepared by bubbling CO_2 into water at 25 °C. The CO_2 concentration was varied from 6 to 24 mM and HCO_3^- concentration from 5 to 90 mM. The CO_2 + H_2O ⇌ HCO_3^- + H^+ equilibrium becomes increasingly shifted toward HCO_3^- at increasing pH, and the pH range above 7.5 is not amenable to studies of the dehydration reaction by the changing pH-indicator assay; likewise, CO_2 hydration cannot be measured below pH 6.2 using this method. The steady-state parameters k_{cat} and k_{cat}/K_m and their standard errors were determined by fitting the observed initial rates (corrected for the uncatalyzed reaction) to the Michaelis−Menten equation. The pH-independent values of k_{cat} and pK_a for CO_2 hydration of Zn− and Co−Cam were determined by fitting the observed pH-dependent steady-state parameters k_{cat} to eq 4

$$k_{cat}^{obs} = k_{cat} (1+10^{(pK_a-pH)}) \qquad (4)$$

and the pH-independent values for k_{cat}/K_m and pK_as for CO_2 hydration of Zn− and Co−Cam by fitting the observed pH-dependent steady-state parameters k_{cat}/K_m to eq 5.

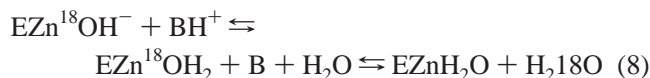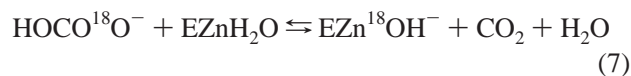$$k_{cat}/K_m obs = (k_{cat}/K_m^I \times 10^{(pK_a^{II}-pH)} + k_{cat}/K_m^{II}) \times$$
$$(1+10^{(pK_a^{II} + pK_a^I-2pH)} + 10^{(pK_a^I-pH)} + 10^{(pK_a^{II}-pH)}) \quad (5)$$

The pH-independent values of k_{cat}/K_m and pK_as for HCO_3^- dehydration of Zn− and Co−Cam were determined by fitting the observed pH-dependent steady-state parameters k_{cat}/K_m to eq 6.

$$k_{cat}/K_m^{obs} = k_{cat}/K_m/(1+10^{(pH-pK_a)}) \qquad (6)$$

The buffer dependence was measured at pH 8.2 by varying the CO_2 concentration from 6 to 24 mM and the TAPS concentration from 5 to 50 mM, maintaining the ionic strength at 0.1 M by addition of sodium sulfate. The observed initial rates were fit to the Michaelis−Menten equation. The solvent isotope effect was measured at pD 8.5 using solutions with final concentrations of >95% D_2O. The pD value was determined by addition of 0.4 to the pH value measured with a pH electrode (31). The CO_2 concentrations were varied from 7 to 27 mM based on saturating solutions of CO_2 in D_2O at 25 °C (38.1 mM). All fits described were done using Kaleidagraph (Synergy Software, Reading, PA).

Oxygen-18 Exchange. Mass spectrometry was used to measure the catalyzed and uncatalyzed rates of exchange of ^{18}O from species of CO_2 into water and the rates of exchange of ^{18}O between ^{12}C-containing and ^{13}C-containing species of CO_2 at chemical equilibrium (32). Equations 7 and 8 show the catalytic pathway for the exchange of ^{18}O from bicarbonate to water. In eq 8, B designates buffer in solution and/or an amino acid side chain in the enzyme.

$$HOCO^{18}O^- + EZnH_2O \rightleftharpoons EZn^{18}OH^- + CO_2 + H_2O \qquad (7)$$

$$EZn^{18}OH^- + BH^+ \rightleftharpoons$$
$$EZn^{18}OH_2 + B + H_2O \rightleftharpoons EZnH_2O + H_2^{18}O \quad (8)$$

Two rates in the catalytic pathway can be determined by this method. The first is R_1 the rate of interconversion of CO_2 and HCO_3^- at chemical equilibrium. Equation 9 expresses the substrate dependence of R_1.

$$R_1/[E] = k_{cat}^{ex}[S]/(K_{eff}^S + [S]) \qquad (9)$$

Here, [E] is the total enzyme concentration, k_{cat}^{ex} is a rate constant for maximal HCO_3^- to CO_2 interconversion, [S] is the substrate concentration of HCO_3^- and/or CO_2, and K_{eff}^S is an apparent substrate binding constant (33). Equation 9 can be used to determine the values of K_{eff}^{ex}/K_{eff}^S when applied to the data for varying substrate concentration, or to determine K_{eff}^{ex}/K_{eff}^S directly from R_1 when [S]≪K_{eff}^S. Under steady-state conditions when [S]≪K_m all enzyme species are at their equilibrium concentrations. Hence, in both theory and practice, $k_{cat}ex/K_{eff}^{CO_2}$ is equivalent to k_{cat}/K_m for CO_2 hydration as measured by steady-state methods (33).

This method also is used to determine R_{H_2O}, the rate of release of water labeled with ^{18}O from the enzyme (eq 8). A proton from a donor group BH^+ converts the zinc-bound hydroxide to zinc-bound water, which readily exchanges with unlabeled water. The ^{18}O label is greatly diluted into the solvent water. The value of R_{H_2O} can be interpreted in terms of the rate constant from a predominant donor group to the zinc-bound hydroxide, according to eq 10 (34), in which k_B is the rate constant for intramolecular proton transfer to the zinc-bound hydroxide, K_B is the ionization constant for the donor group, and K_E is the ionization constant of the zinc-bound water molecule.

$$R_{H_2O}/[E] = k_B/((1 + K_B/[H^+])(1 + [H^+]/K_E)) \quad (10)$$

Table 2: Properties of *Methanosarcina thermophila* Cam, Apo-Cam, Zn−Cam, and Co−Cam

enzyme	specific activity (units/mg)[a]	zinc (per subunit)	cobalt (per subunit)	native molecular mass[b] (kDa)
Cam	720	0.67	<0.01[c]	74 ± 4
apo-Cam	20	0.02	<0.01	70 ± 4
Co−Cam	2020	0.06	1.02	70 ± 4
Zn−Cam	910	0.98	<0.01	74 ± 4

[a] One unit = $(t_0 - t)/t$, where t_0 is the time for the uncatalyzed reaction and t is the time for the catalyzed reaction. [b] Determined by Superose 12 gel filtration. [c] Limit of detection.

An Extrel EMX-200 mass spectrometer and a membrane-inlet permeable to dissolved gases were used to measure the rate of distribution of ^{18}O (*32*). Experiments were carried out in the absence of buffers, unless otherwise indicated, which were not needed to maintain pH since these experiments were carried out at chemical equilibrium.

Analytical. CO_2-hydrating activity was routinely measured at room temperature by using a modification of the electrometric method of Wilbur and Anderson (*35*) as described previously (*1*). Protein concentrations of purified enzyme preparations were estimated using A_{280} and an extinction coefficient (15 990 cm^{-1} M^{-1} based on one subunit) calculated from the deduced amino acid sequence (M_r = 22 900) of the *cam* gene (excluding the putative signal sequence). For metals analysis, protein concentrations were also determined by the Biuret method (*36*) using bovine serum albumin and chicken egg white lysozyme (Sigma) as standards. Both methods agreed well. Metals were determined at the Chemical Analysis Laboratory, University of Georgia, Athens, by inductively coupled plasma atomic emission spectroscopy using a Jarrel Ash Plasma Comp 750 instrument. Dialysis tubing was treated as described (*37*), and buffers were made metal free by adding Chelex 100 (5 g/L, BioRad) and removing it by filtration. Samples were dialyzed at 4 °C against a total of 20 mM potassium phosphate (pH 7.0) for 40−50 h prior to metals analysis.

RESULTS

Preparation of Apo-Cam and Reconstitution with Zn and Co. Apo-Cam was prepared using the denaturant guanidine·HCl and the metal chelator dipicolinic acid. After removal of these compounds and refolding the enzyme, native gel filtration chromatography indicated that apo-Cam is trimeric (Table 2). Carbonic anhydrase activity was recovered by reconstituting apo-Cam with either Zn(II) (Zn−Cam) or Co-(II) (Co−Cam) (Table 2). The specific activities of Cam, apo-Cam, and Zn−Cam were directly proportional to the zinc content (Table 2). These results indicate that Zn is not essential for tertiary integrity and are consistent with a Zn or Co requirement for catalysis.

X-ray Absorption Spectroscopy. The Zn(II) ion of Cam has been shown by X-ray crystallography to be bound to three histidine ligands (*12*). At 2.8 Å resolution, a water molecule was tentatively assigned as a fourth ligand based on the fact that solvent completes the coordination sphere in human CAII and acts as the catalytic group (*13*). Figure 1 displays XAS data for Cam. The Zn K-edge spectrum is reminiscent of imidazole coordination (*4*). This is confirmed by curve fitting analyses (Table 3), which find an average
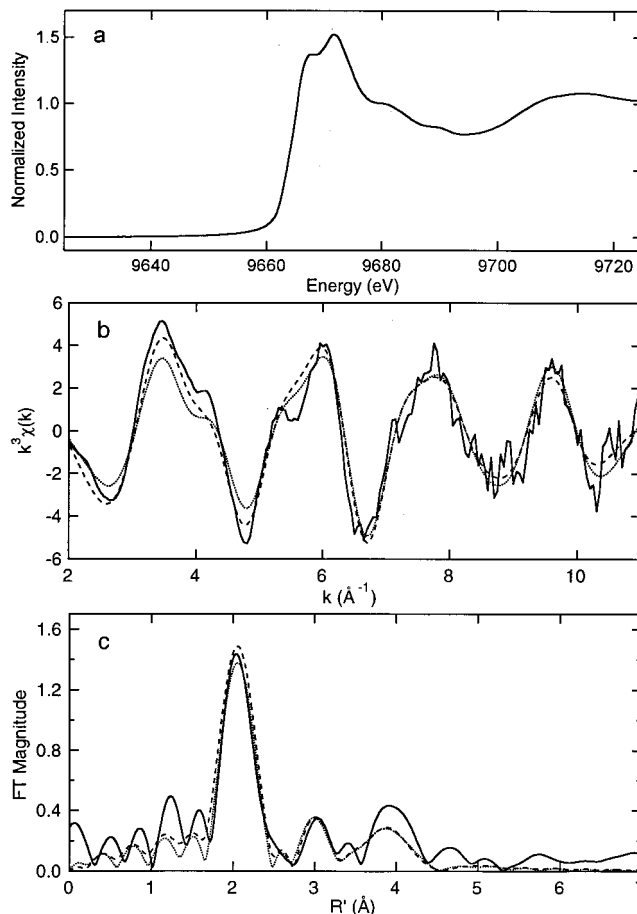

FIGURE 1: −Zn K-edge X-ray absorption spectroscopic data for Cam. The nomalized edge region (a), EXAFS data (b), and Fourier transform (c) for as-isolated Cam (solid line) are compared to fit 1 (shorter dashes) and fit 3 (long dashes) from Table 3.

Zn coordination sphere of Zn(N,O)$_{2-3}$ (imidazole)$_3$. Two EXAFS data simulations are compared to the EXAFS and Fourier transforms of Zn(II)-bound Cam in Figure 1b−c. Both simulations model three imidazole ligands but differ in that fit 1, which mimics the crystal structure, has only water, whereas fit 3 contains three water ligands. Bond valance sum calculations and the goodness of fit for four-, five-, and six-coordinate models with one, two, or three, water molecules respectively, show that the best fit is with three imidazole ligands and five- to six-coordinate Zn. This analysis determines Zn−N(imidazole) and Zn−(N,O) distances of 2.06 Å, which is almost identical to those observed by X-ray crystallography with an average distance of 2.07 Å (*12*). Our survey of structures of Zn(II) complexes containing only N− or O-containing ligands in the Cambridge Structure Database reveals Zn−N distance ranges of 2.00−2.05 Å, 2.07−2.13 Å, and 2.12−2.20 Å for four-, five-, and six-coordinate complexes, respectively. Zn−O distance ranges for similar complexes are 1.85−1.92 Å, 1.98−2.08 Å, and 2.11−2.20 Å. Our EXAFS-derived average Zn−(N,O) distance of 2.06 Å is, therefore, most reminiscent of distances observed in five-coordinate Zn(II) complexes. These EXAFS results are, therefore, in agreement with the X-ray structural assignment of three histidine ligands and further suggests an overall five- or six-coordinate Zn(II) ion in Cam, most likely completed by two or three solvent molecules.

Table 3: Curve-Fitting Results for Zn K-Edge EXAFS of As-Isolated (Zn-Containing) Cam from *Methanosarcina thermophila*[a]

sample	fit	group	shell	N_s	R_{as} (Å)	σ_{as}^2 (Å^2)	ΔE_0 (eV)	f[b]	BVS[c]
as isolated	1	imid + N/O	Zn–N	(4)[d]	2.06	0.0031	−1.78	0.087	1.61
$k = 2.0-11.0$ Å^{-1}		imid	Zn–C$_2$	(3)	[3.02][e]	0.0063	[−1.78]	⟨0.077⟩[f]	
		imid	Zn–N$_3$	(3)	[4.16]	[0.0086]	[−1.78]		
		imid	Zn–C$_4$	(3)	[4.21]	[0.0087]	[−1.78]		
		imid	Zn–C$_5$	(3)	[3.09]	[0.0064]	[−1.78]		
	2	imid + N/O	Zn–N	(5)	2.06	0.0050	−1.91	0.081	2.07
		imid	Zn–C$_2$	(3)	[3.03]	0.0057	[−1.91]	⟨0.071⟩	
		imid	Zn–N$_3$	(3)	[4.16]	[0.0079]	[−1.91]		
		imid	Zn–C$_4$	(3)	[4.21]	[0.0080]	[−1.91]		
		imid	Zn–C$_5$	(3)	[3.09]	[0.0058]	[−1.91]		
	3	imid + N/O	Zn–N	(6)	2.06	0.0067	−2.16	0.081	2.54
		imid	Zn–C$_2$	(3)	[3.03]	0.0062	[−2.16]	⟨0.073⟩	
		imid	Zn–N$_3$	(3)	[4.16]	[0.0085]	[−2.16]		
		imid	Zn–C$_4$	(3)	[4.21]	[0.0086]	[−2.16]		
		imid	Zn–C$_5$	(3)	[3.09]	[0.0063]	[−2.16]		
	4	imid + N/O	Zn–N	(5)	2.06	0.0050	−2.16	0.082	2.16
		imid	Zn–C$_2$	(2)	[3.02]	0.0034	[−2.16]	⟨0.073⟩	
		imid	Zn–N$_3$	(2)	[4.16]	[0.0045]	[−2.16]		
		imid	Zn–C$_4$	(2)	[4.20]	[0.0046]	[−2.16]		
		imid	Zn–C$_5$	(2)	[3.08]	[0.0034]	[−2.16]		
	5	imid + N/O	Zn–N	(6)	2.06	0.0068	−2.31	0.083	2.62
		imid	Zn–C$_2$	(2)	[3.02]	0.0029	[−2.31]	⟨0.074⟩	
		imid	Zn–N$_3$	(2)	[4.16]	[0.0040]	[−2.31]		
		imid	Zn–C$_4$	(2)	[4.20]	[0.0041]	[−2.31]		
		imid	Zn–C$_5$	(2)	[3.08]	[0.0030]	[−2.31]		
	6	imid	Zn–N	(4)	2.06	0.0038	−1.79	0.090	1.53
		imid	Zn–C$_2$	(4)	3.02	[0.0055]	[−1.79]	⟨0.082⟩	
		imid	Zn–N$_3$	(4)	[4.16]	[0.0076]	[−1.79]		
		imid	Zn–C$_4$	(4)	[4.20]	[0.0077]	[−1.79]		
		imid	Zn–C$_5$	(4)	[3.09]	[0.0056]	[−1.79]		

[a] Group is the chemical unit defined for the multiple scattering calculation. N_s is the number of scatterers (or groups) per metal. R_{as} is the metal-scatterer distance. σ_{as}^2 is a mean square deviation in R_{as}. ΔE_0 is the shift in E_0 for the theoretical scattering functions. [b] f is a normalized error (χ-squared): $f = \{\sum_j [k^3(\chi_i^{obs} - \chi_i^{calc})]^2/N\}^{1/2}/[(k^3\chi^{obs})_{max} - (k^{3obs})_{min}]$. [c] BVS $= \sum s$, $s = e^{[(r_o - r)/B]}$, $B = 0.37$, $r_0(Zn^{2+}\text{-}N) = 1.704$, $r_0(Zn^{2+}\text{-}O) = 1.776$, all the N/O ligands were treated as they were nitrogens and thus the values are somewhat underestimated. [d] Numbers in parentheses were not varied during optimization. [e] Numbers in square brackets were constrained to be a multiple of the above value. [f] Numbers in angle brackets are f for the smoothed data.

Figure 2 shows the XAS data for Co—Cam. The Co K-edge spectrum shows a small peak below the edge (ca. 7710 ev; Figure 2a and inset) which has been attributed to the 1s→3d transition (*4*). Qualitatively, the low intensity of this transition and the absence of a transition in the 7720 eV region (assignable to 1s → 4p + shakedown, prominent for square-planar geometries) rule out the possibility of this Co(II) site being four-coordinate (*38, 39*). EXAFS simulation based on four- and six-coordinate models containing three imidazoles are compared with the EXAFS and Fourier transforms of the Co—Cam in Figure 2b—c. From these fits and from bond valance sum calculations (Table 4), the results find an average coordination sphere of Co(N,O)$_3$(imidazole)$_{2-3}$ with average Co—(N,O) distances of 2.09 Å, which suggests that Co(II) has isomorphously replaced Zn(II) in Cam. Standard errors associated with EXAFS-derived distances are ± 0.02 Å.

Visible Absorption Spectroscopy of Co—Cam. In contrast to Zn (II) (3d^{10}), the 3d^7 electronic configuration of Co(II) is accessible to electronic spectroscopic methods. Spectroscopy of Co(II)-substituted human carbonic anhydrase isozymes has been used to probe the active sites (*40, 41*). The visible difference absorption spectrum of Co—Cam *minus* Zn—Cam is shown in Figure 3. The shape of the spectrum has features in common with the low pH (Co(II)—water) form of the Co-(II)-substituted human isozyme CAII, which has been suggested to contain a large percentage of pentacoordinated species (*4, 42*). It is not possible to assign a definite number

of ligands based on the absorption spectrum alone, as the absorption intensity is not only sensitive to the coordination number but also to the geometry of the Co(II) site (*40*); nonetheless, the low maximum extinction coefficient ($\epsilon_{527 nm} = 40$ M^{-1} cm^{-1}) is indicative of a highly coordinated or symmetrical site suggesting that five- or six-coordination is possible and four-coordination is unlikely, results which are consistent with the EXAFS results.

Kinetic Characterization. The pH-dependencies of CO$_2$ hydration and HCO$_3^-$ dehydration catalyzed by Zn— and Co—Cam were measured by stopped-flow spectroscopy using the changing pH-indicator assay. Comparison of Figures 4 and 5 shows that the efficiency (k_{cat}/K_m) of either Zn—Cam or Co—Cam for CO$_2$ hydration was severalfold greater than HCO$_3^-$ dehydration over the physiological pH range of 6.5 to 7.5. At pH 7.0, the difference in efficiency was 10-fold greater. These results are consistent with the proposed physiological function for Cam in which CO$_2$ is hydrated to a charged species outside the cell membrane for thermodynamically favorable removal of CO$_2$ produced in the cytoplasm during growth on acetate (*1*).

The steady-state parameter k_{cat} for CO$_2$ hydration for both Zn— and Co—Cam was pH-dependent with a single pK_a within the range of 6.5—6.8, whereas k_{cat}/K_m was dependent on two ionizations with pK_a values within the range of 6.7—6.9 and 8.2—8.4 (Figure 4, Table 5). These results suggest that there are two ionizable groups in the enzyme that must be deprotonated for maximum efficiency of CO$_2$ hydration;
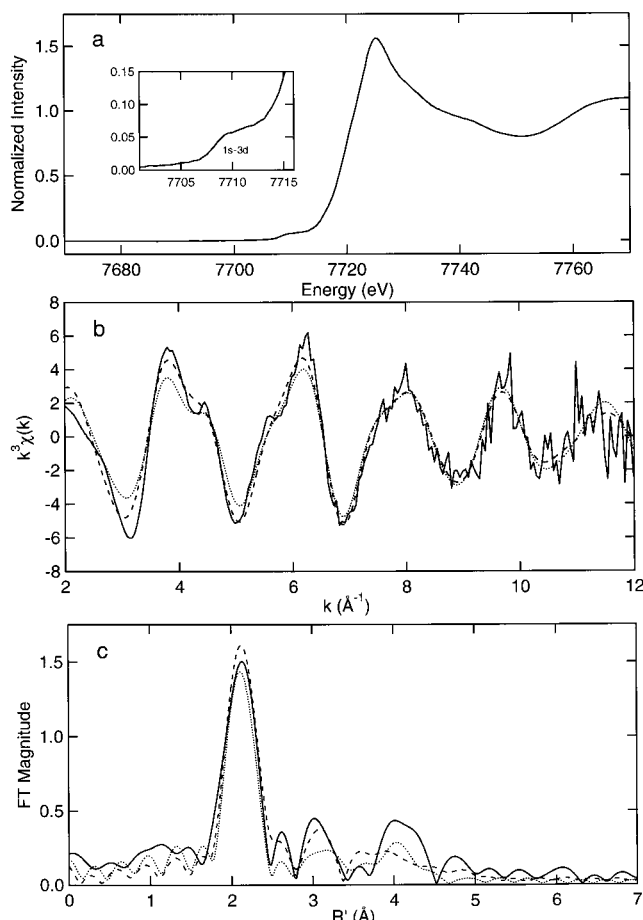
FIGURE 2: −Co K-edge X-ray absorption spectroscopic data for Co−Cam. The normalized edge region (a), EXAFS data (b), and Fourier transform (c) for Cam (solid line) are compared to fit 1 (shorter dashes) and fit 3 (longer dashes) from Table 4. The inset to (a) shows an expanded view of the 1s→3d preedge transition.

however, deprotonation of the ionizable group with the higher pK_a does not result in increased k_{cat}. The pH-dependence of k_{cat}/K_m for HCO_3^- dehydration catalyzed by Zn− or Co−Cam, measured in the range of pH 5.5 to 7.5, indicates a dependency on a single ionizable group with a pK_a similar to the pK_a of 6.7−6.9 determined by the pH-dependence of the Zn− or Co−Cam catalyzed CO_2 hydration (Figure 4, Table 5). Comparison of the pH-dependence of CO_2 hydration for Zn− and Co−Cam indicates that the pK_a values of the two ionizable groups are comparable (Figure 4, Table 5). Furthermore, the K_m values for both enzymes were comparable over the pH range assayed (data not shown). Therefore, it can be assumed that Zn− and Co−Cam follow a similar catalytic mechanism. The values for k_{cat} and k_{cat}/K_m for CO_2 hydration and HCO_3^- dehydration of Co−Cam, however, were approximately 2-fold higher than for Zn−Cam. These results suggest that individual rate constants affecting k_{cat} and k_{cat}/K_m change dependent on the metal ion present in the active site. The rate constant k_{cat}/K_m was also determined for Zn−Cam by measuring the exchange of ^{18}O between species of CO_2 and water (eq 9). The pH-dependence of k_{cat}/K_m determined in this way had a maximal value of $(1.4 \pm 0.1) \times 10^7$ M^{-1} s^{-1} with clear evidence of the influence of two groups, one with a pK_a of 8.1 ± 0.1 and the other less well determined pK_a near 5.7 (Figure 6). R_{H_2O} depends on both the values of pK_a of the zinc-bound

water and of the proton shuttle (*32*), the same groups that are expected to influence k_{cat}/K_m. Thus, two values of pK_a are also found from the pH-dependence of $R_{H_2O}/[E]$, the rate constant for the release of $H_2^{18}O$ from the active site (Figure 7). In this case, the apparent pK_a values were 6.0 ± 0.2 and 8.6 ± 0.2. These values are in general agreement with the pK_a values determined by steady-state analysis with apparent differences in pK_a values the result of the different experimental approaches combined with inherent experimental error.

The dependence of CO_2 hydration catalyzed by Zn−Cam on the concentration of TAPS buffer was determined at pH 8.2. The steady-state parameter k_{cat} was buffer-dependent in a saturable manner with an apparent K_m(TAPS) of 6 mM (Figure 8). These results indicate that buffer acts as a second substrate in a "ping-pong" mechanism, likely accepting a proton from the enzyme during CO_2 hydration. A second-order rate constant for intermolecular proton transfer (k_B) was calculated based on the K_m of effective buffer (the fraction of total buffer in unprotonated form capable of accepting a proton from the enzyme) and the subunit turnover number under buffer-saturating conditions. At pH 8.2, proton-transfer between a single Zn−Cam subunit and 50 mM TAPS buffer ($pK_a = 8.4$) occurred with a rate constant of $k_B = 3 \times 10^7$ M^{-1} s^{-1} and at low buffer concentrations this step was rate-limiting. The rate constant k_{cat}/K_m was not dependent on the concentration of buffer (Figure 8, insert), a result consistent with the human CAII zinc-hydroxide mechanism in which the interconversion of CO_2 and HCO_3^-, reflected in k_{cat}/K_m, is separate from intermolecular proton transfer (*16*). The solvent isotope effect for CO_2 hydration at pH 8.5 catalyzed by Zn−Cam was measured at a concentration of TAPS buffer (50 mM) where intermolecular proton transfer is not rate-limiting. There was no significant isotope effect on the steady-state parameter k_{cat}/K_m (Table 5). This result suggests that no major structural changes in the enzyme are imposed in D_2O and that the catalytic steps up to and including the first irreversible step of the reaction do not contain a rate-contributing proton-transfer step at pH 8.5. The observed solvent hydrogen isotope effect on k_{cat} of 2.6 (Table 5) is smaller than the 3.8 reported for human CAII (*43*), but similar to the value reported for human CAIV (*14*), which follows a similar mechanism as CAII. This result suggests that in Zn−Cam, even under saturating buffer concentrations, proton transfer is partially rate-determining at pH 8.5. No significant change in k_{cat} or k_{cat}/K_m was observed at pH 7.2 over the range of 5 to 50 mM MOPS buffer (data not shown). The changing pH-indicator assay allows reliable measurements only at a total buffer concentration greater than 5 mM; thus, either the K_m(MOPS) is too low to detect or the mechanism and rate-determining step deviate at pH 7.2.

DISCUSSION

Despite the unrelatedness of the α and γ classes of carbonic anhydrases, the active sites of human CAII and Cam share one common feature: both enzymes contain an essential zinc ion coordinated to stereochemically identical nitrogen atoms of the imidazole side chains of three histidine residues (*12*). The spectroscopic results presented here are consistent with two or three water molecules completing the coordination spheres of Zn− and Co−Cam. This result

Table 4: Curve-Fitting Results for Co K-edge EXAFS of Co−Cam from *Methanosarcina thermophila*[a]

sample	fit	group	shell	N_s	R_{as} (Å)	σ_{as}^2 (Å²)	ΔE_0 (eV)	f^b	BVS[c]
Co−Cam $k = 2.0-12.0$ Å^{-1}	1	imid + N/O	Co−N	(4)[d]	2.09	0.0032	4.51	0.094	1.67
		imid	Co−C$_2$	(3)	[3.08][e]	0.0060	[4.51]	⟨0.066⟩[f]	
		imid	Co−N$_3$	(3)	[4.23]	[0.0083]	[4.51]		
		imid	Co−C$_4$	(3)	[4.19]	[0.0082]	[4.51]		
		imid	Co−C$_5$	(3)	[3.14]	[0.0061]	[4.51]		
	2	imid + N/O	Co−N	(5)	2.09	0.0047	3.97	0.086	2.01
		imid	Co−C$_2$	(3)	[3.07]	0.0058	[3.97]	⟨0.057⟩	
		imid	Co−N$_3$	(3)	[4.22]	[0.0080]	[3.97]		
		imid	Co−C$_4$	(3)	[4.18]	[0.0080]	[3.97]		
		imid	Co−C$_5$	(3)	[3.13]	[0.0059]	[3.97]		
	3	imid + N/O	Co−N	(6)	2.09	0.0061	3.43	0.083	2.36
		imid	Co−C$_2$	(3)	[3.07]	0.0057	[3.43]	⟨0.056⟩	
		imid	Co−N$_3$	(3)	[4.22]	[0.0080]	[3.43]		
		imid	Co−C$_4$	(3)	[4.18]	[0.0079]	[3.43]		
		imid	Co−C$_5$	(3)	[3.13]	[0.0059]	[3.43]		
	4	imid + N/O	Co−N	(5)	2.09	0.0047	3.91	0.087	1.91
		imid	Co−C$_2$	(2)	[3.07]	0.0033	[3.91]	⟨0.056⟩	
		imid	Co−N$_3$	(2)	[4.22]	[0.0046]	[3.91]		
		imid	Co−C$_4$	(2)	[4.18]	[0.0045]	[3.91]		
		imid	Co−C$_5$	(2)	[3.13]	[0.0034]	[3.91]		
	5	imid + N/O	Co−N	(6)	2.09	0.0062	3.40	0.084	2.25
		imid	Co−C$_2$	(2)	3.07	0.0032	[3.40]	⟨0.055⟩	
		imid	Co−N$_3$	(2)	[4.21]	[0.0044]	[3.40]		
		imid	Co−C$_4$	(2)	[4.17]	[0.0044]	[3.40]		
		imid	Co−C$_5$	(2)	[3.13]	[0.0033]	[3.40]		
	6	imid	Co−N	(4)	2.09	0.0036	4.22	0.096	1.78
		imid	Co−C$_2$	(4)	[3.07]	[0.0052]	[4.22]	⟨0.071⟩	
		imid	Co−N$_3$	(4)	[4.22]	[0.0072]	[4.22]		
		imid	Co−C$_4$	(4)	[4.18]	[0.0071]	[4.22]		
		imid	Co−C$_5$	(4)	[3.13]	[0.0053]	[4.22]		

[a] Group is the chemical unit defined for the multiple scattering calculation. N_s is the number of scatterers (or groups) per metal. R_{as} is the metal-scatterer distance. σ_{as}^2 is a mean square deviation in R_{as}. ΔE_0 is the shift in E_0 for the theoretical scattering functions. [b] f' is a normalized error (χ-squared): $f = \{\sum_j[k^3(\chi_i^{obs} - \chi_i^{calc})]^2/N\}^{1/2}/[(k^3\chi^{obs})_{max} - (k^{3obs})_{min}]$. [c] BVS = $\sum s$, $s = e^{[(r_o-r)/B]}$, $B = 0.37$, $r_0(Co^{2+}-N) = 1.79$, $r_0(Co^{2+}-O) = 1.692$. The r_0 for Co^{2+}−N was interpolated using experimental published values for Mn, Fe, Cu, and Zn. For all nonimidazole ligands a solvent molecule (oxygen) was used as r_0. [d] Numbers in parentheses were not varied during optimization. [e] Numbers in square brackets were constrained to be a multiple of the above value. [f] Numbers in angle brackets are f for the smoothed data.
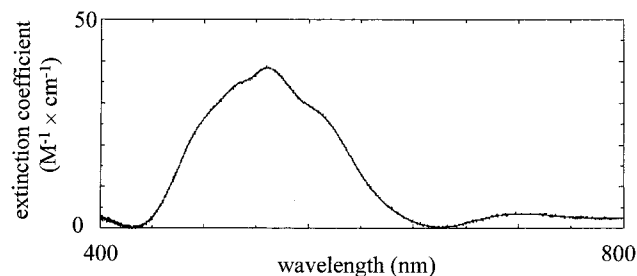

FIGURE 3: Optical absorption difference spectrum (Co− *minus* Zn−Cam). Conditions were 1.1 mM Cam in 20 mM MOPS, pH 7.0 at 25 °C.

FIGURE 4: pH dependence of CO$_2$ hydration catalyzed by Zn−Cam and Co−Cam. CO$_2$ hydrase activity for Zn−Cam (○, □) and Co−Cam (●, ■) were measured in 50 mM buffer at 0.1 M ionic strength and 25 °C. The subunit concentrations used were 0.4−0.6 μM for Zn−Cam and 0.2−0.3 μM for Co−Cam, respectively. The CO$_2$ concentration was varied from 6 to 24 mM. The pH-independent rate constants and pK_as were derived from fitting the observed steady-state parameters k_{cat} (○, ●) to eq 4 and k_{cat}/K_m (□, ■) to eq 5. Data were weighted based on the standard errors determined by fitting the observed initial rates to the Michaelis−Menten equation. Results of those fits are listed in Table 5.

contrasts with human CAII in which a single water molecule completes the tetrahedral coordination of zinc. The values of k_{cat}/K_m and k_{cat} for CO$_2$ hydration catalyzed by Cam increase with increasing pH, suggesting that an unprotonated form of the enzyme is required for catalytic competence consistent with nucleophilic attack of a hydroxyl group on CO$_2$. The pH profiles of k_{cat}/K_m determined by the changing pH indicator and ^{18}O exchange assays indicate the dependence on at least two ionizable groups, one with a pK_a value within the range 6.0−6.9 and a second within the range of 8.1−8.4. At high pH (pH > 8), neither a buffer dependence nor solvent hydrogen isotope effect on k_{cat}/K_m was observed for Zn−Cam. These results indicate that the proton-transfer step(s) (eqs 3a and 3b) are separate from the catalytic steps (eqs 2a and 2b) reflected in k_{cat}/K_m, which rules out zinc-bound hydroxide acting as a general base to extract a proton
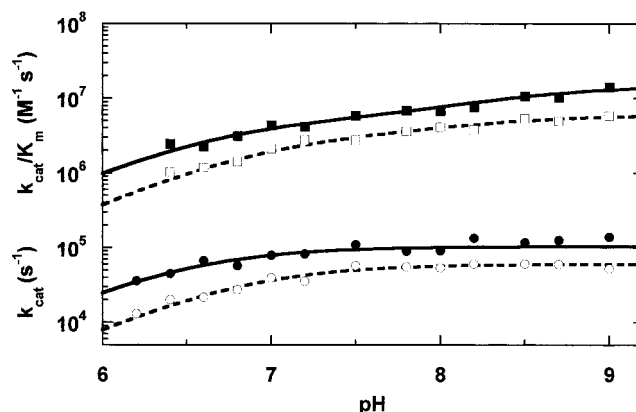
from nascent water as the source of the attacking hydroxyl (*16*). Therefore, at pH values above the higher pK_a, the catalysis of Cam appears to follow the zinc hydroxide mechanism, as first described for human CAII (*16, 17*).

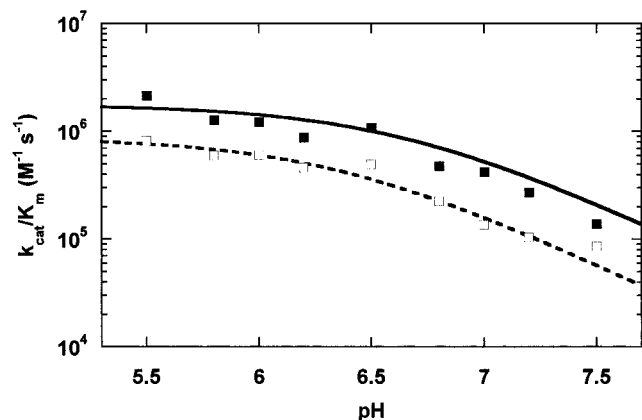FIGURE 5: pH dependence of HCO_3^- dehydration catalyzed by Zn—Cam and Co—Cam. HCO_3^- dehydrase activity for Zn—Cam ($\square$) and Co—Cam ($\blacksquare$) were measured in 50 mM buffer at 0.1 M ionic strength and 25 °C. The subunit concentrations used were 0.7—3.0 μM for Zn—Cam and 0.3—1.3 μM for Co—Cam, respectively. The HCO_3^- concentration was varied from 5 to 90 mM. The pH independent rate constants and pK_a values were derived by fitting the observed steady-state parameters k_{cat}/K_m to eq 6. Data were weighted based on the standard errors determined by fitting the observed initial rates to the Michaelis—Menten equation. Results of those fits are listed in Table 5.

Table 5: pH-Independent Steady-State Kinetic Parameters Derived from the pH-Dependence of CO_2 Hydration and HCO_3^- Dehydration Catalyzed by Zn—Cam and Co—Cam from *Methanosarcina thermophila*

	Zn—Cam	Co—Cam
CO_2 hydration[a]		
k_{cat} ($\times 10^{-4}$ s^{-1})	6.1 ± 0.1	10.4 ± 0.2
pK_a	6.8 ± 0.1	6.5 ± 0.1
$k_{cat}(H_2O)/k_{cat}(D_2O)$	2.6 ± 0.2	ND[b]
$k_{cat}/K_m^{\ I}$ ($\times 10^{-6}$ M^{-1} s^{-1})	3.3 ± 0.5	5.3 ± 0.5
$pK_a^{\ I}$	6.9 ± 0.1	6.7 ± 0.1
$k_{cat}/K_m^{\ II}$ ($\times 10^{-6}$ M^{-1} s^{-1})	6.1 ± 0.5	15.1 ± 1.4
$pK_a^{\ II}$	8.2 ± 0.3	8.4 ± 0.2
$k(H_2O)/k(D_2O)$	0.9 ± 0.1	ND
HCO_3^- dehydration[c]		
k_{cat} ($\times 10^{-4}$ s^{-1})	>5.1	>10.0
k_{cat}/K_m ($\times 10^{-6}$ M^{-1} s^{-1})	0.87 ± 0.02	1.76 ± 0.03
pK_a	6.3 ± 0.1	6.6 ± 0.1

[a] pH-Independent kinetic parameters and pK_a values for CO_2 hydration (calculated per subunit) were determined in the range of pH 6.2—9.0, in 50 mM buffer, 25 °C, ionic strength 0.1 M, using the changing pH-indicator assay as described under Materials and Methods. The solvent hydrogen isotope effect was measured at pH/D 8.5. [b] pH-Independent kinetic parameters and pK_as for HCO_3^- dehydration (calculated per subunit) were determined in the range of pH 5.5—7.5, in 50 mM buffer, 25 °C, ionic strength 0.1 M, using the changing pH-indicator assay as described under Materials and Methods. Non-Michaelis—Menten behavior was observed at high bicarbonate concentrations due to a change in pK_a of the indicator during the assay caused by variation of ionic strength at high bicarbonate concentrations. The pH-independent values for k_{cat} are, therefore, lower limits and a pK_a could not be determined.

The first half-reaction of the sequential catalytic mechanism of human CAII is the interconversion of CO_2 and HCO_3^- by direct nucleophilic attack of the zinc hydroxide (with a pK_a of 7) on CO_2, followed by replacement of HCO_3^- by water at the active site (eqs 2a and 2b). Kinetically, these steps are reflected in k_{cat}/K_m that in human CAII has a pH profile revealing the pK_a of the zinc-bound water. Assuming metal-bound hydroxide is the catalytic group in Cam, it is not yet clear which of the two reported pK_a values for $k_{cat}/$
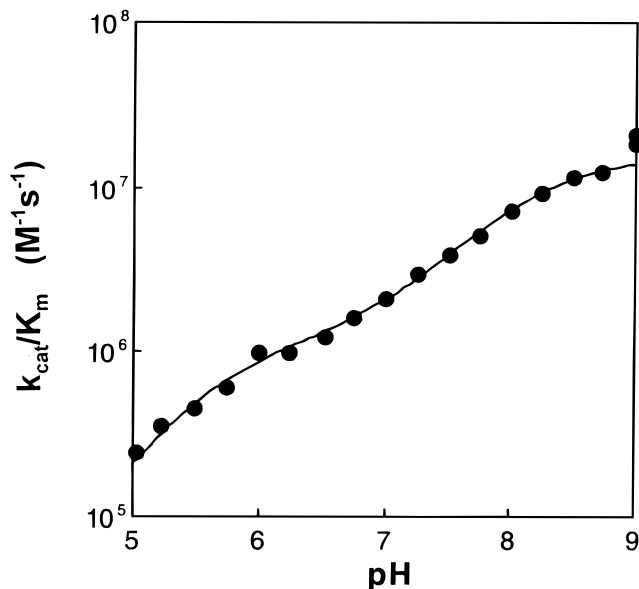

FIGURE 6: The pH dependence of k_{cat}/K_m determined for Zn—Cam by ^{18}O exchange at 25 °C. The total concentration of all species of CO_2 was 25 mM and the total ionic strength of solution was maintained at 0.2 M by addition of Na_2SO_4. No buffers were used. The solid line is a least-squares fit to the sum of two ionizations with one pK_a at 8.1 ± 0.1 and a second at 5.7 ± 0.2 and a maximum of $k_{cat}/K_m = (1.4 ± 0.1) \times 10^7$ M^{-1} s^{-1}.
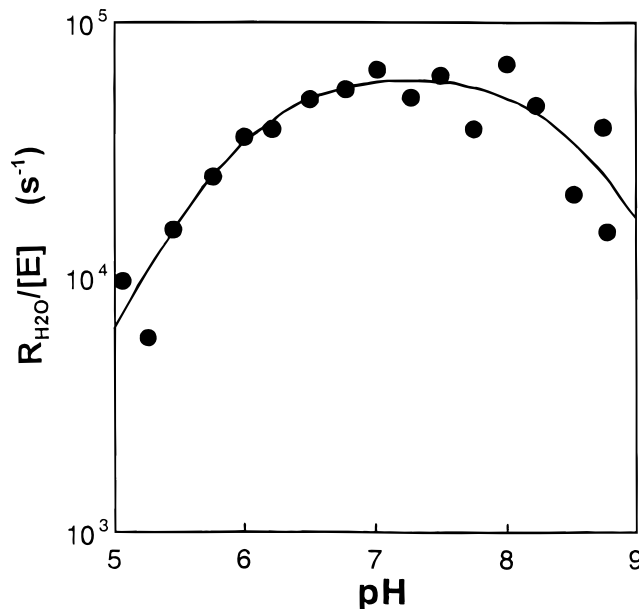

FIGURE 7: The pH dependence of $R_{H_2O}/[E]$, the rate of release from Zn—Cam of $H_2^{18}O$. Conditions were as described for Figure 1. The solid line is a least-squares fit of eq 4 to the data yielding two values of pK_a, 6.0 ± 0.2 and 8.6 ± 0.2. The value of the rate constant for proton transfer to the active site is dependent on the assignment of these values of pK_a, as described in the text.

K_m reflect the ionization of metal-bound water. Theoretically, there should be a difference in the pK_a for ionization of the metal-bound water between Zn— and Co—Cam. For human CAII this difference is approximately 0.3 units (44); however, the data in Figure 4 were fit to two ionizable groups with pK_a values only 2 units apart, which excludes the resolution of differences between Zn— and Co—Cam for either the high or low pK_a values. Assuming a zinc hydroxide mechanism, the pK_a of the zinc hydroxide can be estimated as 6.8—7 from the ratio of k_{cat}/K_m for CO_2 hydration and HCO_3^-
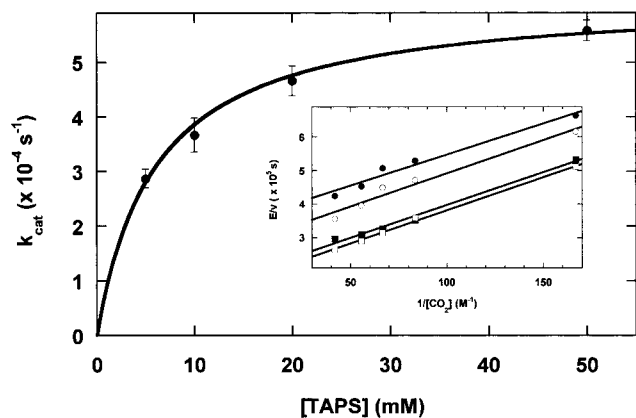
FIGURE 8: Buffer dependence of CO_2 hydration catalyzed by as-isolated heterologously produced Cam. CO_2 hydrase activity (0.7 μM, subunit concentration) was measured at pH 8.2, ionic strength 0.1 M, and 25 °C. CO_2 concentration was varied from 6 to 24 mM and TAPS concentration from 5 to 50 mM. The observed steady-state parameters k_{cat} were fitted to the Michaelis–Menten equation: K_m(TAPS) = 6.1 ± 0.9 mM, k_{cat}max = 6.2 (± 0.3) × 10^4 s^{-1}. Data were weighed based on the standard errors for k_{cat} (shown) determined by fitting the observed initial rates to the Michaelis–Menten equation. Insert: double reciprocal plot of observed initial velocities versus CO_2 concentration at different concentrations of TAPS buffer: ● 5 mM, ○ 10 mM, ■ 20 mM, □ 50 mM.

dehydration and the apparent dissociation constant for H_2CO_3 (6.3 × 10^7) using the Haldane relationship (eq 11) (*43, 45, 46*).

$$K_a (H_2CO_3)/K_a (ZnH_2O) =$$
$$k_{cat}/K_m (CO_2)/k_{cat}/K_m (HCO_3^-) \quad (11)$$

The observation of two pK_a values in the pH profile of k_{cat}/K_m for hydration could be due to either: (i) kinetic perturbation of the pK_a of the zinc-bound water caused by both a "sticky" substrate (CO_2) and a "sticky" proton (such as mechanism 65 in ref 47), or (ii) ionization of a second group that affects k_{cat}/K_m. Although we cannot completely distinguish between these two mechanisms with the current data, the kinetic data on other carbonic anhydrases indicate that CO_2 is not a sticky substrate and CO_2 dissociation is rapid compared to CO_2 hydration (*14–17*), suggesting that the first mechanism is unlikely. For the second mechanism, the additional pK_a could reflect the ionization of (i) a nearby residue that either modestly enhances the binding of CO_2 or the rate constant for the product formation in k_{cat}/K_m without increasing the rate constant for k_{cat} (proton transfer) (*47*), or (ii) the proton shuttle exerting an effect on the pK_a of the zinc-bound water. This second explanation is consistent with results of the α-carbonic anhydrases in which k_{cat}/K_m for esterase function of human CAII at low sulfate concentrations reveals the presence of a second ionization, probably that of His64 (*48*). Furthermore, for α-carbonic anhydrases the affinity of CO_2 is very weak (0.1 M) with no observable pH-dependence (*49*). Moreover, in mammalian CAV the replacement of Tyr64 with His changes the pH profile of k_{cat}/K_m for hydration of CO_2 from that described by a single ionization to that consistent with two ionizations (*15*).

In the first half-reaction of the sequential mechanism for the human isozyme CAII (eqs 2a and 2b), the interconversion of CO_2 and HCO_3^- approaches the diffusion-controlled limit and does not contain rate-determining proton-transfer steps

(*17, 33*). The second half-reaction is the ionization of the zinc-bound water (eqs 3a and 3b). Release of the proton from the active site and completion of the catalytic cycle is rate-limiting and reflected in k_{cat} (10^6 s^{-1}). The single pK_a observed in the pH profile for k_{cat} for the hydration of CO_2 is consistent with the mechanism of eqs 2 and 3 and reflects the pK_a of an intramolecular proton shuttle that accepts a proton from the zinc-bound water. Such properties are observed for human CAII in which His64 is the proton shuttle (*13*). Buffer facilitates the release of the proton from human isozyme CAII, and at saturating buffer concentration, the intramolecular proton transfer from zinc-bound water to the proton shuttle group His64 is rate-determining (*19, 50*). At pH 8.2, buffer (TAPS) facilitates proton transfer in Zn–Cam (Figure 8). This, along with the solvent isotope effect on k_{cat} at saturating buffer concentrations, indicates that proton transfer is a significant rate-contributing step of the maximal velocity. The value of k_{cat}/K_m for TAPS as a second substrate in the catalysis is 3 × 10^7 M^{-1} s^{-1} (Figure 8). This value is far from the diffusion-controlled limit (10^9 M^{-1} s^{-1}), suggesting that the group, which donates a proton to TAPS, is not readily accessed by this buffer. Such a group might be a proton shuttle, similar to the role of His64 in CAII, or it might be the zinc-bound water itself. The pH-dependence of $R_{H_2O}/[E]$, the rate constant for release of $H_2^{18}O$ from the enzyme shows the effects of two residues with values of pK_a determined at 8.6 ± 0.2 and 6.0 ± 0.2. These values of pK_a represent a proton acceptor group, the zinc-bound hydroxide, and one (or more) proton donor group(s). When assumed that the pK_a near 6.0 is that of the zinc-bound water and that near 8.6 is the donor group(s), we obtain a value of (6.5 ± 0.6) × 10^4 s^{-1} for k_B of eq 10, the rate constant for intramolecular proton transfer from the donor group(s) to the zinc-bound water. This is close to the value for k_{cat} for dehydration (Table 5) and is, therefore, consistent with the steady-state data. However, if we reverse the pK_a assignments so that 8.6 is the pK_a of the zinc-bound water, then k_B = (2.5 ± 1.5) × 10^7 s^{-1}, which is not consistent with the steady-state data and is very much larger than the value of k_B near 10^6 s^{-1} for human CAII, one of the most efficient of the CAs from the α class. Hence, these considerations suggest that the pK_a of the zinc-bound water in Zn–Cam is near 6.0, in approximate agreement with the application of the Haldane equation. The cause of the difference of about one pK_a unit in the stopped-flow and ^{18}O-exchange estimates of this pK_a is uncertain but is under further investigation. The pK_a near 8.6 may represent proton shuttles of higher pK_a as found in carbonic anhydrase V (*15*).

SUPPORTING INFORMATION AVAILABLE

Major fits for both Zn and Co EXAFS were redone using only k = 4.0–12.0 $Å^{-1}$ data. Although the goodness-of-fit indicies (fN) improve as would be expected for the shorter k range, the essential results (distances and DeBye–Waller factors) are insignificantly different from those determined by analysis of the k = 2.0–12.0 D^{-1} range. This material is available free of charge via the Internet at http://pubs.acs.org.

REFERENCES

1. Alber, B. E., and Ferry, J. G. (1994) *Proc. Nat. Acad. Sci. U.S.A. 91*, 6909–6913.

2. Fukuzawa, H., Suzuki, E., Komukai, Y., and Miyachi, S. (1992) *Proc. Natl. Acad. Sci. U.S.A. 89*, 4437−4441.

3. Hewett-Emmett, D., and Tashian, R. E. (1996) *Mol. Phylogenet. Evol. 5*, 50−77.

4. Yachandra, V., Powers, L., and Spiro, T. G. (1983) *J. Am. Chem. Soc. 105*, 6596−6604.

5. Bracey, M. H., Christiansen, J., Tovar, P., Cramer, S. P., and Bartlett, S. G. (1994) *Biochemistry 33*, 13126−13131.

6. Rowlett, R. S., Chance, M. R., Wirt, M. D., Sidelinger, D. E., Royal, J. R., Woodroffe, M., Wang, Y. F. A., Saha, R. P., and Lam, M. G. (1994) *Biochemistry 33*, 13967−13976.

7. Boriack-Sjodin, P. A., Heck, R. W., Laipis, P. J., Silverman, D. N., and Christianson, D. W. (1995) *Proc. Natl. Acad. Sci. U.S.A. 92*, 10949−53.

8. Eriksson, A. E., and Liljas, A. (1993) *Proteins 16*, 29−42.

9. Hakansson, K., Carlsson, M., Svensson, L. A., and Liljas, A. (1992) *J. Mol. Biol. 227*, 1192−1204.

10. Kannan, K. K., Notstrand, B., Fridborg, K., Lovgren, S., Ohlsson, A., and Petef, M. (1975) *Proc. Natl. Acad. Sci. U.S.A. 72*, 51−5.

11. Stams, T., Nair, S. K., Okuyama, T., Waheed, A., Sly, W. S., and Christianson, D. W. (1996) *Proc. Natl. Acad. Sci. U.S.A. 93*, 13589−94.

12. Kisker, C., Schindelin, H., Alber, B. E., Ferry, J. G., and Rees, D. C. (1996) *EMBO J. 15*, 2323−2330.

13. Lindskog, S. (1997) *Pharmacol. Ther. 74*, 1−20.

14. Baird, T. T., Waheed, A., Okuyama, T., Sly, W. S., and Fierke, C. A. (1997) *Biochemistry 36*, 2669−2678.

15. Heck, R. W., Boriack-Sjodin, P. A., Qian, M. Z., Tu, C. K., Christianson, D. W., Laipis, P. J., and Silverman, D. N. (1996) *Biochemistry 35*, 11605−11611.

16. Silverman, D. N., and Lindskog, S. (1988) *Acc. Chem. Res. 21*, 30−36.

17. Steiner, H., Jonsson, B.-H., and Lindskog, S. (1975) *Eur. J. Biochem. 59*, 253−259.

18. Hurt, J. D., Tu, C., Laipis, P. J., and Silverman, D. N. (1997) *J. Biol. Chem. 272*, 13512−8.

19. Tu, C. K., Silverman, D. N., Forsman, C., Jonsson, B. H., and Lindskog, S. (1989) *Biochemistry 28*, 7913−8.

20. Johansson, I. M., and Forsman, C. (1994) *Eur. J. Biochem. 224*, 901−907.

21. Johansson, I.-M., and Forsman, C. (1993) *Eur. J. Biochem. 218*, 439−446.

22. Tatusov, R. L., Koonin, E. V., and Lipman, D. J. (1997) *Science 278*, 631−7.

23. Alber, B. E., and Ferry, J. G. (1996) *J. Bacteriol. 178*, 3270−3274.

24. Scott, R. A. (1985) *Methods Enzymol. 117*, 414−458.

25. Bear, C. A., Duggan, K. A., and Freeman, H. C. (1975) *Acta Crystallogr., Sect. B 31*, 2713.

26. Prince, E., Mighell, A. D., Reimann, C. W., and Santoro, A. (1972) *Cryst. Struct. Commun. 1*, 247.

27. Brown, I. D., and Altermatt, D. (1985) *Acta Crystallogr. 1341*, 244−247.

28. Liu, W., and Thorp, H. H. (1993) *Inorg. Chem. 32*, 4102−4105.

29. Thorp, H. H. (1992) *Inorg. Chem. 31*, 1585−1588.

30. Khalifah, R. G. (1971) *J. Biol. Chem. 246*, 2561−73.

31. Schowen, K. B., and Schowen, R. L. (1982) *Methods Enzymol. 87*, 551−606.

32. Silverman, D. N. (1982) *Methods Enzymol. 87*, 732−52.

33. Simonsson, I., Jonsson, B. H., and Lindskog, S. (1979) *Eur. J. Biochem. 93*, 409−17.

34. Silverman, D. N., Tu, C. K., Chen, X., Tanhauser, S. M., Kresge, A. J., and Laipis, P. J. (1993) *Biochemistry 32*, 10757−10762.

35. Wilbur, K. M., and Anderson, N. G. (1948) *J. Biol. Chem. 176*, 147−154.

36. Gornall, A. G., Bardawill, C. J., and David, M. M. (1948) *J. Biol. Chem. 177*, 751−766.

37. Auld, D. S. (1988) *Methods Enzymol. 158*, 13−14.

38. Wirt, M. D., Sagi, I., Eefei, C., Frisbie, S. M., Lee, R., and Chance, M. (1991) *J. Am. Chem. Soc. 113*, 5299−5304.

39. Wirt, M. D., Kumar, M., Wu, J. J., Scheuring, E. M., Ragsdale, S. W., and Chance, M. R. (1995) *Biochemistry 34*, 5269−5273.

40. Bertini, I., Canti, G., Luchinat, C., and Borghi, E. (1983) *J. Inorg. Biochem. 18*, 221−9.

41. Lindskog, S. (1966) *Biochemistry 5*, 2641−6.

42. Koenig, S. H., Brown, R. D., Bertini, I., and Luchinat, C. (1983) *Biophys J. 41*, 179−87.

43. Steiner, H., Jonsson, B. H., and Lindskog, S. (1976) *FEBS Lett. 62*, 16−20.

44. Kogut, K. A., and Rowlett, R. S. (1987) *J. Biol. Chem. 262*, 16417−24.

45. Pocker, Y., and Janjic, N. (1987) *Biochemistry 26*, 2597−606.

46. Segel, I., H. (1975) Enzyme Kinetics, Wiley-Interscience, New York.

47. Cleland, W. W. (1977) *Adv. Enzymol. 45*, 273−387.

48. Simonsson, I., and Lindskog, S. (1982) *Eur. J. Biochem. 123*, 29−36.

49. Riepe, M. E., and Wang, J. H. (1968) *J. Biol. Chem. 243*, 2779−87.

50. Taoka, S., Tu, C. K., Kistler, K. A., and Silverman, D. N. (1994) *J. Biol. Chem. 269*, 17988−17992.